# 13 Light Scattering by Particles and Defects on Surfaces: Semiconductor Wafer Inspection

B.M. Nebeker and E.D. Hirleman

Department of Mechanical and Aerospace Engineering
Arizona State University
Box 876106. Tempe, AZ 85287-6106. U.S.A.
nebeker@coolmail.com, hirleman@asu.edu

**Abstract.** Nonintrusive optical techniques for accurate sizing of discrete particles (or bubbles) suspended in continuous media have been studied for years and have reached, for some applications, an advanced stage of development. In contrast, a related problem of considerable importance that has received less attention is that of accurate characterization of fine particles or other features/defects on and under surfaces. This capability is much needed in the fields of semiconductor and integrated circuit fabrication, digital storage media manufacturing, and for research on contamination of optical components for both earth- and space-based applications. In this presentation, we show the development of theoretical based scattering modeling and comparisons between our experimental and theoretical studies of light scattering by features on and under surfaces relevant to semiconductor wafer inspection. The experimental work shown here involves measurements of angle-resolved light scattering signatures (for 64 scattering angles) from an individual spherical particle 0.482 $\mu$m in diameter on a bare Si wafer. Experiments and predictions show good agreement, and the models are being used in predicting the performance of wafer scanners for various experimental conditions and for assisting in the design of future-generation surface defect characterization instruments.

## 1 Introduction

Integrated circuit chips have an ever increasing effect on almost every aspect of life, and technology continues to dictate that the smallest, or critical, dimensions of these IC's reach into the smaller and smaller regions of the nanoscale. This trend presents the semiconductor industry a manufacturing challenge to produce smaller and more densely packed integrated circuitry. With smaller circuitry, particle contamination and manufacturing defects must be more closely controlled to avoid loss in production yield. The challenge to the manufacturer is to produce chips in a contamination-free environment with as few defects as possible. This increasing emphasis on improving chip manufacturing yield is very critical since the amount of capital investment involved is immense and competition is fierce.

With the increasing number of devices, the smallest dimension of leading-edge production devices has decreased to well below 0.2 $\mu$m. A rule-of-thumb in the industry states that a "killer" contaminant which may render a chip

F. Moreno and F. González (Eds.): Lectures 1998, LNP 534, pp. 237−252, 2000.

useless is one-third to one-half the size of the chip critical dimension. [1] The critical dimension of a "killer" defect is projected to decrease to 0.06 $\mu$m in 2001 and 0.02 $\mu$m in 2006. [1]

It is imperative to detect particle contamination and defects that appear during the manufacturing process. Contamination may come from equipment, non-clean environments, and the workers themselves. Defects and contamination also result from unsatisfactory photolithography and etching processes which involve the addition or removal of material on the chips. With proper detection of contamination and defects, manufacturing problems can be isolated and their causes corrected quickly. Failure to detect defects and contamination may result in significant losses in production yield and profits. Surface scanning inspection systems ($SSIS$) are used to detect particle contamination and manufacturing defects. Generally, to detect surface features, these inspection systems measure scattered light from laser beams that are incident upon wafer substrates. Information about the features can be deduced from the pattern and magnitude of the scattered light irradiance. The size, shape, and material of a scatterer as well as the wavelength and polarization of the incident beam affect the characteristics of the scattered light.

Increasing demand for more accurate and sensitive detection systems caused by the decreasing critical IC dimensions has led to the development of new, non-intrusive detection systems. Development of new systems requires large investments of capital, thus careful efforts in the design process must be taken to ensure good return on investment. Development of new systems can be approached by two methods. In one method, careful light scattering experiments may be conducted in a laboratory environment to determine scattering characteristics from semiconductor wafer defects and the requirements for optimum detector design. The advantage of this approach is that it provides a physical environment that may be similar to the actual manufacturing environment, and these conditions can be quantified as part of the experiment. The disadvantages of this approach are the high costs for careful experiments, and the limitations to provide results that encompass the entire range of features, defects, substrates, and detector systems that exist in manufacturing. For this reason, an alternative approach for inspection tool design is to develop software to model the light scattering and detection systems. The advantages of this approach are that a wide range of variables can be studied quickly and a smaller amount of capital investment is usually needed as compared to experiment. The software could be used by a large number of modelers resulting in wider range of results than could possibly be conducted under experimental conditions. The disadvantages of this approach include the difficulty to determine the model accuracy and the ability to account for unknown parameters which may exist in the manufacturing environment. The best approach for the design of detection systems is to utilize the experimental and numerical approaches in conjunction with each other. If conducted simultaneously, experiments can be used to quantify the

accuracy of the numerical codes, and the numerical codes can be used to determine the accuracy of the experiments conducted.

In this study, we will first provide a background into the study of scattering from features on surfaces. A review of numerical methods used to predict scattering from features is given, and a history of scattering experiments for features on surfaces will be given. Next, development of the discrete-dipole approximation (DDA) method to model light scattering from features on surfaces is described. Predictions of this method will then be compared to scattering experiments performed at Arizona State University on features found on semiconductor wafers.

## 2 Literature Survey

This section provides a survey of literature associated with numerical modeling of light scattering from features on surfaces and experimental procedures used to measure scattering.

### 2.1 Numerical Modeling

The road leading to the development of numerical methods to model electromagnetic scattering from a wide range of features of any shape has been paved by elementary methods developed for specific cases, but whose accuracy and range of applicability are too limited for the needs of the semiconductor industry. Early models investigated scattering from isolated particles with no surface interaction. As early as the turn of this century, scientists investigated light scattering from dust particles to explain their effect on the color of the sky. Lorenz in 1890 [2] and Mie in 1908 [3] independently developed analytical methods based on Maxwell's equations to determine light scattering by a sphere in the presence of an electromagnetic plane wave. The analytical methods employed the Bessel and Hankel functions, which were difficult to compute accurately before the use of computers as mathematical tools became practical during the 1960's.

The advent of powerful computers allowed rigorous modeling of Maxwell's equations to be possible. Peltoniemi [4] provides a detailed discussion of numerical approaches for the electromagnetic scattering problem. Most numerical techniques involve the discretization of the scattering volume, applying Maxwell's equations to each sub-volume of the scatterer, creating a set of algebraic equations. One family of these discretization numerical methods include the finite-element and finite-difference methods. When applied to the Maxwell equations, very large but sparse matrices are solved [5,6]. While the sparseness of the matrices provides a modeling advantage, disadvantages lie in the difficulty to determine and apply correct boundary conditions for the problem. Non-standard procedures are often needed for these methods, and these procedures may lead to uncertainty of the modeling accuracy [7].

Another Maxwell equation based model is the volume integral equation technique [4]. This technique includes a family of closely related methods where the volume of the scatterer is divided into a number of sub-volumes approximated with uniform internal fields where point matching techniques are used to solve for the fields within these sub-volumes. Several methods based on this technique are known as the volume integral equation formulation ($VIEF$) method [8], the method of moments ($MoM$) [9,10], the digitized Green's function method ($DGFM$) [11], and the discrete-dipole approximation ($DDA$) method, also known as the coupled-dipole method [12,13]. The cells of the scatterer created by these methods are considered as dipoles. In these methods, a number of dipoles are positioned in a lattice to model the volume, shape, and composition of a scattering feature. The electric field at each dipole includes contributions from the incident beam field, the field reflected from the surface, and the field created by superposition of the fields from each dipole on the lattice. The solution procedure determines the electric field at each point in the lattice. Basically, the only mathematical difference between the methods of the volume integral equation family is in the way by which the matrix diagonal elements, called the dipole polarizabilities in the DDA method, are approximated. Peltoniemi describes the differences among the volume integral equation methods that, during their development, the DDA methods emphasize the role of dipoles as radiating physical units, while the MoM/VIEF/DGFM methods consider dipoles as abstract mathematical tools without any deeper meaning, replaceable with anything which appears better in terms of modeling [4]. For a more detailed discussion of the relationship between the DDA method and the MoM method, refer to the works of Lakhtakia [14,15].

The progression of light scattering modeling from features in free-space to features in the presence of an interacting surface leads to more detailed and complicated models. The interacting surface complicates the scattering problem, as the surface boundary conditions modify the scattered field characteristics. Development of models for features in the presence of interacting surfaces followed the same path taken by free-space modeling - first, restrictive analytical models were developed, and as the study of light scattering progressed, methods based more rigorously on Maxwell's equations were developed. Some of the first models for features on surfaces were based on the Lorenz-Mie theory for light scattering from spherical features with flat surface interaction using plane-wave expansions of the scattered field [16,17]. Particle contaminants on wafer substrates in the semiconductor industry generally are not spherical, so the Lorenz-Mie formulation may not provide predictions with acceptable accuracy. Another method to compute scattering from features on surfaces uses the exact image theory to model features above a perfect conductor [18,19]. Most substrates in the semiconductor industry are not perfect conductors, and the features were confined to be spherical when using this theory, so other approaches need to be considered. In 1995,

Videen[20] developed a model for arbitrarily shaped features above a conducting surface. Wojcik et al. [21] and Liswith [22] have used the time-domain finite-element method for Maxwell's equations to model scattering from features on surfaces. Along with discretizing the scatterer when developing the model, the interacting surface is discretized as part of the surrounding medium. With this method, application of the boundary conditions can be very difficult and the computational requirements are significant.

Several methods of the volume integral equation technique have been applied to the electromagnetic scattering problem with surface interaction. One of the most recent models developed is called the discrete-source method (DSM) which entails the use of linear combinations of fields from dipoles and multipoles to solve Maxwell's equations and the boundary conditions [23]. Recently Ivakhnenko and Eremin have proposed a VIEF model for features above surfaces [24].

The numerical method discussed in detail for this study is the discrete-dipole approximation (DDA) when the surface boundary interaction is applied. Taubenblatt [25,26] modified the free-space DDA method by employing the Sommerfeld integrals for dipole radiation above an interacting surface. At Arizona State University, Schmehl [27] and Nebeker [28] developed a DDA model with surface interaction (DDSURF) inspired by the free-space DDA code developed by Draine and Flatau [29] (DDSCAT). A two-dimensional Fast Fourier Transform was introduced to reduce the number of computational operations required to solve the matrix equations of the model [30]. A post-processor (RDSURF) was developed by Nebeker et al. [31] which used the computed internal scatterer field to compute the far-field scattering. The development of DDSURF has been conducted concurrently with experiments conducted at ASU and comparisons have been made between experiment and numerical prediction [31–33].

### 2.2 Experimental Measurements

Weber conducted some of the first careful experimental measurements of angle-resolved scattering by individual particles on bare surfaces [34]. Light scattering from polystyrene latex (PSL) spheres on a nickel substrate was measured. Weber compared the experimental results to a model that used the Lorenz-Mie theory for a spherical particle above a surface with angle resolved measurements of light scattered from different sized PSL spheres on silicon substrates. Bawolek [35] extended the work of Weber by investigating other sizes of PSL spheres, and different substrate materials. Warner [36] continued the work using the Arizona State University Scatterometer and investigated the effect of feature refractive index on the far-field scattering by considering different scatterers. This was an important extension to the work by Bawolek [34] because, in the semiconductor industry, most detection systems are calibrated using standard PSL spheres, but since most contamination during the semiconductor manufacturing process is not from PSL

features. Contamination may result from features composed of aluminum, silicon dioxide, tungsten, etc., and calibration to determine contaminant size based on PSL spheres may give misleading results. The materials that Warner studied included silicon dioxide, tungsten, aluminum and silicon. Starr [37] brought this work to fruition with the investigation of light scattering from features more representative of what is found in the semiconductor industry. These features composed of silicon dioxide material on silicon wafers were present on the Arizona State University/Semiconductor Research Corporation (ASU/SRC) section of the SEMATECH Patterned Wafer Defect Standard (PWDS) developed by Scheer of VLSI Standards, Inc. [31–33,38]. The structures were simple enough for accurate characterization by numerical scattering models, and generally represented structures typically found in the semiconductor industry.

## 3 The Discrete-Dipole Approximation Method

In this section, we discuss the development of the discrete-dipole approximation (DDA) method used here to model the scattering from features. In the DDA method, a lattice of dipoles is used to model features present on or near a surface. The feature shape is modeled by the arrangement of the dipoles, and the physical properties of the feature are modeled by designating the polarizeability of each dipole. Figure 1 shows a dipole lattice configuration for a spherical particle on a surface.

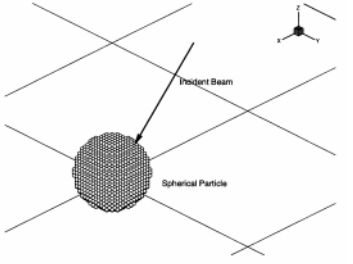


**Fig. 1.** Dipole configuration for a spherical particle on a surface.

### 3.1 Internal Field Computation

When an electrical field is applied to the dipoles, dipole moments are induced at each dipole. At a dipole $i$, the dipole moment $\boldsymbol{p}_i$ is related to the total electrical field $\boldsymbol{E}_{tot,i}$by the dipole polarizeability $\alpha_i$ through

$$\overrightarrow{p_i} = \alpha_i \overrightarrow{E}_{tot,i} \tag{1}$$

Recently, considerable effort has been taken in the development of the polarizeability model used for the DDA. Draine and Goodman [39] discuss several models. The lattice dispersion relation (LDR) is the version which has been most recommended for accuracy.

The total electrical field at the dipole $i$, $\boldsymbol{E}_{tot,i}$, is the summation of the incident field - including the direct beam field and the beam field reflected from the surface, $\boldsymbol{E}_{inc,i}$, the field by direct interaction between the dipoles in the lattice, $\boldsymbol{E}_{dir,i}$, and the dipole fields reflected from the surface, $\boldsymbol{E}_{ref,i}$. Substituting the summation of the fields into 1 and rearranging, we get

$$(\alpha_i)^{-1} \overrightarrow{p_i} - \overrightarrow{E}_{dir,i} - \overrightarrow{E}_{ref,i} = \overrightarrow{E}_{inc,i} \tag{2}$$

The electrical field by direct interaction between the dipoles, $\boldsymbol{E}_{dir,i}$, can be represented as

$$\overrightarrow{E}_{dir,i} = \frac{k_o^2}{\varepsilon_o} \sum_{j=1, j\neq i}^{N} \bar{G}_{ij} \overrightarrow{p}_i \tag{3}$$

where $\bar{G}_{ij}$ is the dyadic Green's function [30], and $N$ is the total number of dipoles in the lattice.

The electrical field interaction between dipoles with reflection from the surface, $\boldsymbol{E}_{ref,i}$, can be represented as

$$\overrightarrow{E}_{ref,i} = \frac{k_o^2}{\varepsilon_o} \sum_{j=1}^{N} \left( \overline{S}_{ij} + \frac{k_o^2}{\varepsilon_o} \frac{k_1^2 - k_2^2}{k_1^2 + k_2^2} \bar{G}_{ij}^I \right) \overrightarrow{p}_i \tag{4}$$

The components of the $3x3$ matrix are given by the Sommerfeld integral terms as described in Nebeker [28]. The Sommerfeld integral terms are computed numerically using routines developed by Lager and Lytle, [38] where $k_1$and $k_2$ are the wave numbers in the above surface medium and substrate medium, and $\varepsilon_o$ is the permittivity of the medium surrounding the scatterer. $\bar{G}_{ij}^I$ is the image dyadic Green's function.

It is possible to represent the summation equations in terms of matrix equations consisting of $N$ dipoles. The matrix equation for the entire problem can be represented as

$$\left(\overline{B} + \overline{A} + \overline{R}\right) \overline{P} = \overline{E}_{inc} \tag{5}$$

For $N$ total dipoles, $\overline{B}$ is the diagonal matrix of the inverse of the polarizabilities

$$\overline{B} = diag(\alpha_{1x}^{-1}, \alpha_{1y}^{-1}, \alpha_{1z}^{-1}, ..., \alpha_{Nx}^{-1}, \alpha_{Ny}^{-1}, \alpha_{Nz}^{-1}) \tag{6}$$

and $\overline{A}$ is the matrix that corresponds to (4) which is for direct interaction between the dipoles and $\overline{R}$ is the matrix that corresponds to (4) for the dipole reflected field interaction. $\overline{A}$ and $\overline{R}$ each consists of $N^2$ $3x3$ submatrices

$$\overline{A} = \begin{bmatrix} \overline{A}_{11} \ ... \ \overline{A}_{1N} \\ \\ \overline{A}_{N1} \ ... \ \overline{A}_{NN} \end{bmatrix}, \qquad \overline{R} = \begin{bmatrix} \overline{R}_{11} \ ... \ \overline{R}_{1N} \\ \\ \overline{R}_{N1} \ ... \ \overline{R}_{NN} \end{bmatrix} \tag{7}$$

where $\overline{A}_{ij}$ and $\overline{R}_{ij}$ are submatrices representing each dipole-dipole interaction Green's functions. These submatrices are described in Schmehl et. al [30]. $\overline{P}$, the dipole moment vector, and $\overline{E}_{inc}$, incident field vector, are composed of $N$ $1x3$ vectors:

$$\overline{P} = [\boldsymbol{p}_1 ... \boldsymbol{p}_N]^T, \qquad \overline{E}_{inc} = [\boldsymbol{E}_{inc,1} ... \boldsymbol{E}_{inc,N}]^T \tag{8}$$

where $\boldsymbol{p}_i$ is the dipole moment vector at dipole $i$, and $\boldsymbol{E}_{inc,i}$ is the incident field vector at dipole $i$.

The solution procedure needed to solve for $\overline{P}$ in (5) usually requires an iterative method. Direct inversion of the matrix $\left(\overline{B} + \overline{A} + \overline{R}\right)$ to solve (5) is impractical if large number of dipoles are required to model the scattering feature. A major concern when using the $DDA$ method is the iterative procedure used to solve the system of dipole equations. Draine [13] used a complex conjugate gradient ($CCG$) method to solve the system of equations for a free space scattering features. The range in which accurate convergence to a solution could be obtained was determined to be a function of the relation of the dipole spacing used to the wavelength of the incident electromagnetic wave within the scatterer. Thus, as the refractive index of a scatterer increased, decreasing the wavelength within the scatterer, the dipole spacing must be decreased. With the introduction of a scattering surface, the condition of the governing matrix relation is modified and convergence using a general $CCG$ method developed for symmetric matrices may not be achieved. It became necessary to find other iterative procedures that allowed for convergence to be achieved more readily, even as the condition becomes worse and the matrix becomes less symmetric. Nebeker et. al [41] studied of several methods for the $DDA$ method with surface interaction. It was found that the quasi-minimal residual ($QMR$) method of Freund [42] provided better convergence characteristics when compared to the $CCG$ method and the bi-conjugate gradient ($BCG$) method.

### 3.2 Far-Field Computation

The dipole moment distribution within the scattering feature, $\overline{P}$, is used to determine the scattering response in the far-field. In this section, we show how to compute the scattered field from dipoles above a surface by separating the

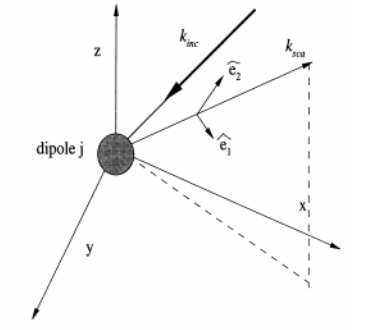


**Fig. 2.** Geometrical configuration for far-field scattering.

scattering into two components: the field direct from the dipole to the point of observation, and the field from the dipole to the point of observation which is reflected from the surface.

The basis of this analysis is that the point of detection of the scattered field is in the far-field region. The far-field can be defined by the following conditions:

$$|\boldsymbol{r}_i| >> |\boldsymbol{r}_j| \qquad \text{and} \qquad k_2 \, |\boldsymbol{r}_i| \, \sqrt{\varepsilon} >> 1 \tag{9}$$

where $\boldsymbol{r}_j$ is the radiating dipole position vector, and $\boldsymbol{r}_i$ is the point of observation. Equation (9) describes the far-field at $\boldsymbol{r}_i$ is at a distance far from the scatterer (at $\boldsymbol{r}$) when compared to the scattered field wavelength.

Application of these far-field limitations to the Maxwell equations leads to the relation for the direct scattered field from $N$ dipoles to the far field at $\boldsymbol{r}_i$:

$$\overrightarrow{E}_{sca,dir}\left(\boldsymbol{r}_i\right) = k_2^2 \frac{\exp(ik_2 r_i)}{4\pi r_i} \sum_{j=1}^{N} \exp(-i\boldsymbol{k}_{sca}\boldsymbol{r}_j) \left[\overline{I} - \hat{e}_r\hat{e}_r\right] \overrightarrow{p}_j \tag{10}$$

The dyad vector $\hat{e}_r\hat{e}_r$ projects the vector $\boldsymbol{p}_j$ in the direction perpendicular to $\hat{e}_r$. These projections can be represented in spherical $\theta$ and $\phi$ components, or they can be resolved in the scattering frame $(\hat{e}_1, \hat{e}_2, \hat{e}_3)$ shown in Fig. 2. When the scattering field of (10) is decomposed into the scattering frame, we get

$$\overrightarrow{E}_{sca,dir}\left(\boldsymbol{r}_i\right) = k_2^2 \frac{\exp(ik_2 r_i)}{4\pi r_i} \sum_{j=1}^{N} \exp(-i\boldsymbol{k}_{sca} \cdot \boldsymbol{r}_j) \left[(\boldsymbol{p}_j \cdot \hat{e}_1)\, \hat{e}_1 + (\boldsymbol{p}_j \cdot \hat{e}_2)\, \hat{e}_2\right] \tag{11}$$

For the field components that have been reflected from the surface, the far-field can be approximated using the reflection coefficient approximation ($RCA$), which models the scattered wave interaction with the surface by using the Fresnel reflection coefficients. The equation for this reflected field can be based on the equivalent of 11, and including the Fresnel coefficients is

$$\overrightarrow{E}_{sca,ref}\left(\boldsymbol{r}_i\right) = k_2^2 \frac{\exp(ik_2 r_i)}{4\pi r_i} \times \sum_{j=1}^{N} \exp(-i\boldsymbol{k}_{I,sca} \cdot \boldsymbol{r}_j) \left[R^{TM}\left(\boldsymbol{p}_j \cdot \hat{e}_1\right)\hat{e}_1 + R^{TE}\left(\boldsymbol{p}_j \cdot \hat{e}_2\right)\hat{e}_2\right] \tag{12}$$

where $\boldsymbol{k}_{I,sca} = (k_{sca,x}, k_{sca,y}, -k_{sca,z})$ is the image scattering direction wave vector. $R^{TM}$ and $R^{TE}$ are the transverse magnetic ($TM$) and transverse electric ($TE$) Fresnel reflection coefficients respectively.

By summing the direct and reflected scattered far-field contributions, $\boldsymbol{E}_{sca,dir}$ and $\boldsymbol{E}_{sca,ref}$, from each of the $N$ dipoles, the field at an observation point $i$ is

$$\overrightarrow{E}_{sca}\left(\boldsymbol{r}_i\right) = k_2^2 \frac{\exp(ik_2 r_i)}{4\pi r_i} \times \sum_{j=1}^{N} \left\{ \begin{array}{c} \exp(-i\boldsymbol{k}_{sca} \cdot \boldsymbol{r}_j)\left[\left(\boldsymbol{p}_j \cdot \hat{e}_1\right)\hat{e}_1 + \left(\boldsymbol{p}_j \cdot \hat{e}_2\right)\hat{e}_2\right] + \\ \exp(-i\boldsymbol{k}_{I,sca} \cdot \boldsymbol{r}_j)\left[R^{TM}\left(\boldsymbol{p}_j \cdot \hat{e}_1\right)\hat{e}_1 + R^{TE}\left(\boldsymbol{p}_j \cdot \hat{e}_2\right)\hat{e}_2\right] \end{array} \right\} \tag{13}$$

Experimental results for scattering from the features on surfaces are collected in the form of differential scattering cross-section, $dC_{sca}/d\Omega$. Differential scattering cross-section is defined as the energy scattered per unit time per unit solid angle about a certain direction. Bohren and Huffman [44] derived an expression for this:

$$\frac{dC_{sca}}{d\Omega} = \lim_{\Omega \to 0}\left(\frac{C_{sca}}{\Omega}\right) \approx \frac{I_{sca}A}{I_{inc}\left(A/r^2\right)} = \frac{r^2 I_{sca}}{I_{inc}} \tag{14}$$

where $I_{sca}$ is the scattered irradiance, $A$ is the detection area, $r$ is the distance from the feature to the observation point, $I_{inc}$ is the incident irradiance, and $\Omega$ is the detection solid angle.

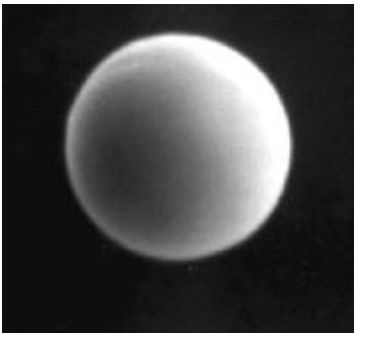

**Fig. 3.** SEM photograph of a spherical particle on a substrate.

# 4 Application of the DDA Method and Comparison with Experimental Results

## 4.1 Feature Characterization/Dipole Moment Distribution Prediction

In this section, we discuss the prediction of the differential scattering cross-section of a scattering spherical feature on a flat substrate shown in Fig. 3. We then compare the predictions to experimental results found at Arizona State University. The scattering feature considered is a 0.482 $\mu$m diameter polystyrene latex ($PSL$) sphere on a silicon surface. The polarized and monochromatic illuminating beam is $p$ - polarized ($TM$), has a wavelength of 632.8 nm, and is directed at a 45° angle from the surface normal. The first step in the modeling process is to determine the lattice arrangement for the dipoles needed to represent the spherical feature. To accurately model the internal field of a scatterer, an element (dipole) spacing of less than one-tenth of the internal field wavelength within the scatterer is required. For a 632.8 nm wavelength, $PSL$ has a refractive index of 1.59, therefore, to satisfy the modeling requirement, the dipole spacing should be less than

$$d_{\max} = 0.1\lambda/\left|n_{part}\right| = 0.1\left(0.6328\mu m\right)/1.59 = 0.04\mu m \tag{15}$$

For the case considered, the $x$, $y$, and $z$ axes of the sphere was filled out by 20 dipoles as shown in Fig. 1, thus a dipole spacing of 0.0241 $\mu$m was used, significantly smaller than the maximum allowable spacing. Fewer dipoles could be used to satisfy the dipole spacing requirements, but the larger number allows a more accurate approximation of the spherical shape when using the rectangular lattice array spacing.

To recap, the input parameters required to arrange the dipole lattice include the feature size, refractive index, and incident beam wavelength. Once the dipole lattice has been arranged, the surface can be characterized by

designating the refractive index of the surface material. The refractive index of a silicon substrate at a 632.8 nm wavelength is $(3.88, 0.023)$. The incident beam is further characterized by indicating the polarization ($p$ or $s$), as well as the incident direction vector. Once these parameters are designated, the dipole matrix equation, (5), can be solved, predicting the internal dipole moment distribution of the scatterer, $\overline{P}$, and then the far-field scattering quantities can be found.

### 4.2 Far-Field Prediction

Once the dipole moment distribution is found using an iterative matrix solution process, the scattered electric far-field can be found. The scattering feature - detector system configuration must be known to solve (13). The scatterer - detector arrangement used for this study is shown in Figs. 4(a) and 4(b). The circular detector, approximately 1 inch in diameter, consists of 32 ring-shaped and 32 wedge-shaped photodetectors. The center of the concentric ring detectors are at angles ranging from 0.6° to 62.7° from the specular scattering direction, 45° from the surface normal vector. The wedge detectors range in the $\phi$ direction from $-90°$ to 90° from the center. The center of the detector is placed 8.2 mm from the scattering feature. The different shaped detectors are used to determine different scattering characteristics. Results from the ring region provide information about the size of the scattering feature, and the wedge section results can provide information about the feature shape.

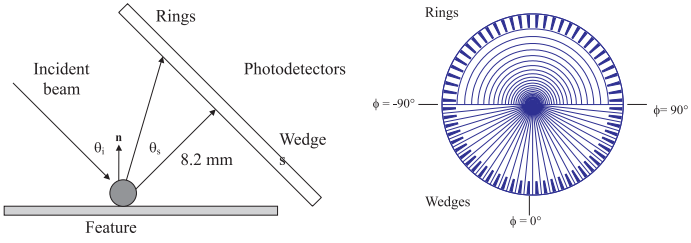


**Fig. 4.** (a) Feature/detector configuration used to determine scattering characteristics (side view). (b) Ring/Wedge detector configuration.

Computationally, the scattered parameters are determined at discrete points, $\boldsymbol{r}_i$ using (13), though the actual ring and wedge detectors occupy finite areas. To approximate the detector response, the electric field is computed at a number of points that lie within the detector region. These fields are then integrated throughout a single detector region (one ring or one wedge), and the integrated result is considered to be the equivalent predicted field measured by a detector.

Figures 5(a) and 5(b) show comparisons of the numerical predictions and experimental differential scattering cross-section results for the ring and wedge detection regions respectively. We see that the predictions and experimental results are in good agreement. In the ring region, the predictions are 5% to 60% higher than experiment, while in the wedge region agreement between prediction and experiment are within 50%. In the semiconductor industry, agreement within these ranges are considered to very good, considering all the factors which may cause variation between experiment conditions and conditions applied to the numerical model. Experimental uncertainties such as beam power, beam width, and detector/feature separation distance can account for the difference between experiment and prediction. For example, when a symmetrical scattering feature such as the sphere is considered, we would expect the wedge data to be symmetrical about the $\phi = 0°$ angle in Fig. 5(b). However, the experimental results are slightly non-symmetric about $\phi = 0°$. One reason for the non-symmetry may be that the alignment of the photodetector was not exactly perpendicular to the plane of beam incidence. Other causes could be deviation of the sphere diameter from the specification of the manufacturer, and/or the presence of an oxide layer due to exposure of the surface to the environment.

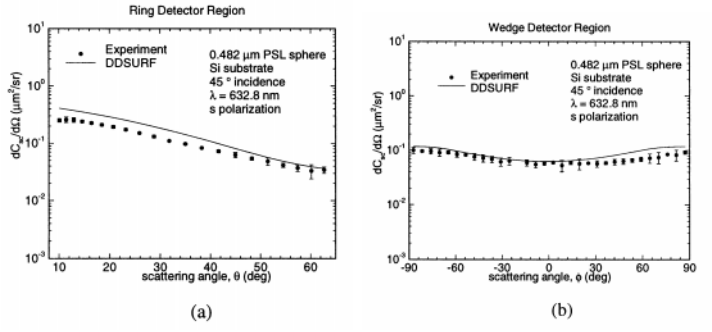


**Fig. 5.** Differential Scattering Cross-Section, comparisons between experimental results and numerical predictions: (a) ringed region; (b) wedge region. Measurements by Starr [37].

## 5 Conclusions

The objective of this work is to show that a numerical model based on the *DDA* method can accurately model scattering from features on surfaces. The models using the *DDA* method are being used in the semiconductor industry to help in the development and calibration of surface scanning inspection systems used in the manufacturing of semiconductor products. Other comparisons between experimental work and the numerical predictions of the *DDA*

method for features on surfaces have been made at Arizona State University. [28, 30, 31, 32, 33, 37] These references show that with careful experimental procedures and accurate modeling, the scattering characteristics of features on surfaces can be accurately predicted using the *DDA* method.

## References

1. Semiconductor Industry Association (1997) The national technology roadmap for semiconductors. SIA, San Jose, CA
2. Lorenz, LV (1890) Upon the light refracted by a transparent sphere. Vidensk. Selsk. Shrifter 6:1-62
3. Mie, G (1908) Considerations on the optics of turbid media, especially colloidal metal sols. Ann D Physik 25:377-442
4. Peltoniemi, JI (1996) Variational volume integral equation method for electromagnetic scattering by irregular grains. J Quant Spectrosc Radiat Transfer, 55:637-647
5. Taflove, A (Winter 1995) Reinventing electromagnetics: Emerging applications for FD-TD computation. IEEE Comp. Science Eng 24-34
6. Patterson, JE, Cwik, T, Ferraro, RD, Jacobi, N, Liewer, PC, Lockhart, TG, Lyzenga, G, Parker, JW, Simoni, DA (1990) Parallel computation applied to electromagnetic scattering and radiation analysis. Electromagnetics 10:21-39
7. Volakis, JL, Chatterjee, A, Gong, J, Kempel, LC, Ross, DC (1994) Progress on the application of the finite element method to 3D electromagnetic scattering and radiation. COMPEL 13A:359-364
8. Hage, JI, Greenberg, JM, Wang, RT (1991) Scattering from arbitrarily shaped particles: Theory and experiment. Applied Optics 30:1141-1152
9. Harrington, RF (1968) Field computation by moment methods in electromagnetics. McGraw-Hill, New York
10. Livesay, DE, Chen, KM (1974) Electromagnetic fields induced inside arbitrarily shaped dielectric bodies. IEEE Trans. Microwave Theory Tech 22:1273-1280
11. Goedecke, GH, O'Brien, SG (1988) Scattering by irregular inhomogeneous particles via the digitized Green's function algorithm. Appl Opt 27:2431-2438
12. Purcell, EM, Pennypacker, CR (1973) Scattering and absorption of light by nonspherical dielectric grains. Astrophys J 186:705-714
13. Draine, BT, Flatau, PJ (1994) The discrete-dipole approximation for scattering calculations. J Opt Soc Am A 11:1491-1499
14. Lakhtakia, A (1993) Strong and weak forms of the method of moments and the coupled dipole method for scattering of time-harmonic electromagnetic fields. Int J Mod Phys C 3:583-603; errata (1993) 4:721-722
15. Lakhtakia, A, Mulholland, GW (1993) On two numerical techniques for light scattering by dielectric agglomerated structures. J Res Natl Inst Stand Technol 98:699-716
16. Bobbert, PA, Vlieger, J (1986) Light scattering by a sphere on a substrate. Physica 137A:213-214
17. Assi, FI (1990) Electromagnetic wave scattering by a sphere on a layered substrate. Master's Thesis, University of Arizona, Tucson, AZ

18. Lindell, IV, Sihvola, AH, Muinonen, KO, Barber, PW (1991) Scattering by a small object close to an interface. I. Exact-image theory formulation. J Opt Soc Am A 8:472-476
19. Johnson, BR (1992) Light scattering from a spherical particle on a conducting plane: I. Normal incidence. J Opt Soc Am A 9:1341-1351
20. Videen, G (1995) Light scattering from a particle on or near a perfectly conducting surface. Optics Comm 115:1-7
21. Wojcik, GL,Vaughn, DK, Galbraith, LK (1987) Calculation of light scatter from structures on silicon Surfaces Lasers in Microlithography Proc. SPIE 774:21-31
22. Liswith, ML (1994) Numerical modeling of light scattering by individual submicron spherical particles on optically smooth semiconductor surfaces. Master's Thesis, Arizona State University, Tempe, AZ
23. Yeremin, YA, Orlov, NV, Sveshnikov, AG (1995) The analysis of complex diffraction problems by the discrete-source method. Comp Math Phys 35:731-743
24. Ivakhnenko, VI, Eremin, YA (1997) Silicon wafer defects analysis. Nonaxisymmetrical model. In: Eremin, YA, Wriedt, T (eds) Electromagnetic and light scattering theory and applications: Proceedings from the 1st workshop on electromagnetic and light scattering: Theory and applications. Moscow State University, Moscow pp 132-134
25. Taubenblatt, MA (1990) Light Scattering from cylindrical structures on surfaces. Optics Letters, 15:255-257
26. Taubenblatt, MA, Tran, TK (1993) Calculation of light scattering from particles and structure by the coupled-dipole method. J Opt Soc Am A 10:912-919
27. Schmehl, R (1994) The coupled-dipole method for light scattering for light particles on plane surfaces. Department of Mechanical and Aerospace Engineering, Arizona State University and the Institut für Thermische Strömungsmaschinen, Universität Karlsruhe, Germany
28. Nebeker, BM (1998) Modeling of light scattering from features above and below surfaces using the discrete-dipole approximation, Ph.D. Dissertation, Arizona State University, Tempe, AZ
29. Draine, BT, Flatau, PJ (1994) The discrete-dipole approximation for scattering calculations. J Opt Soc Am A 11:1491-1499
30. Schmehl, R., Nebeker, BM, Hirleman, ED (1997) The coupled-dipole method for scattering by particles on surfaces using a two-dimensional fast Fourier transform technique. J Opt Soc Am A 14:3026-3036
31. Nebeker, BM, Starr, GW, Hirleman, ED (1995) Light scattering from patterned surfaces and particles on surfaces. In: Lowell, JK, Chen, RT, Mathur, JP (eds) Optical characterization techniques for high performance microelectronic device manufacturing II: Proc SPIE 2638:274-284
32. Nebeker, BM, Schmehl, R, Starr, GW, Hirleman, ED (1996) Prediction of light scattering characteristics of particles and structures on surfaces by the coupled-dipole method. In: Jones, S (ed) Metrology, inspection, and process control for microlithography X: Proc SPIE. 2725:690-697
33. Nebeker, BM, Starr, GW, Hirleman, ED (1996) Prediction of light scattering from structures with particle contaminants. In: Stover, JC (ed) Flatness, roughness, and discrete defect characterization for computer disks, wafers, and flat panel displays: Proc SPIE. 2862:139-150
34. Weber, DC (1986) Light scattering by micron and submicron spheres on optically smooth surfaces. Master's Thesis, Arizona State University, Tempe, AZ

35. Bawolek, EJ (1992) Light scattering by spherical particles on semiconductor surfaces. Ph.D. Dissertation, Arizona State University, Tempe, AZ
36. Warner, TL (1994) Characterization of light scatter by particles of various refractive indices on semiconductor surfaces. Master's Thesis, Arizona State University, Tempe, AZ
37. Starr, GW (1997) Light scattering by submicron particles and defects on smooth and patterned surfaces. Ph.D. Dissertation, Arizona State University, Tempe, AZ
38. Starr, GW, Hirleman, ED (1996) Comparison of experimentally-measured differential scattering cross sections of PSL spheres on flat and patterned surfaces. In: Stover, JC (ed) Flatness, roughness, and discrete defect characterization for computer disks, wafers, and flat panel displays: Proc SPIE. 2862:130-138
39. Draine, BT, Goodman, J (1993) Beyond Clausius-Mossotti: Wave propagation on a polarizable point lattice and the discrete dipole approximation. Astrophys. J 405:685-697
40. Lager, DL, Lytle, RJ (1975) Fortran Subroutines for the Numerical Evaluation of Sommerfeld Integrals unter Anterem, Rep. UCRL-51821. Lawrence Livermore Laboratory, Livermore, CA
41. Nebeker, BM, Starr, GW, Hirleman, ED (1998) Evaluation of iteration methods used when modeling scattering from features on surfaces using the discrete-dipole approximation. J Quant Spectrosc Radiat Transfer 60:493-500
42. R. W. Freund, RW (1992) Conjugate gradient-type methods for linear systems with complex symmetric coefficient matrices. SIAM J Scient and Stat Comp 13:425–448
43. Goodman, JJ, Draine, BT, Flatau, PJ (1991) Application of fast-Fourier-transform techniques to the discrete-dipole approximation. Optics Letters 16:1198-1200
44. Bohren, CF, Huffman, DR (1983) Absorption and Scattering of Light by Small Particles. John Wiley and Sons, New York